Building a functional connectome of the ***Drosophila*** central complex

Romain Franconville[1], Celia Beron[1], and Vivek Jayaraman[1]

[1]Janelia Research Campus, HHMI

April 6, 2018

Abstract

The central complex is a highly conserved insect brain region composed of morphologically stereotyped neurons that arborize in distinctively shaped substructures. The region has been implicated in a wide range of behaviors, including navigation, motor control and sleep, and has been the subject of several modeling studies exploring its circuit computations. Most studies so far have relied on assumptions about connectivity between neurons in the region based on their overlap in light-level microscopic images. Here, we present an extensive functional connectome of *Drosophila melanogaster*'s central complex at cell-type resolution. Using simultaneous optogenetic stimulation, GCaMP recordings and pharmacology, we tested the connectivity between over 70 presynaptic-to-postsynaptic cell-type pairs. The results reveal a range of inputs to the central complex, some of which have not been previously described, and suggest that the central complex has a limited number of output channels. Additionally, despite the high degree of recurrence in the circuit, network connectivity appears to be sparser than anticipated from light-level images. Finally, the connectivity matrix we obtained highlights the potentially critical role of a class of bottleneck interneurons of the protocerebral bridge known as the Δ7 neurons. All data is provided for interactive exploration in a website with the capacity to accommodate additional connectivity information as it becomes available. Raw data and code are made available as an OpenScienceFramework project.

Introduction

Positioned in the middle of the insect brain, the central complex provides a unique opportunity to obtain mechanistic insights into the way brains build and use abstract representations (Turner-Evans and Jayaraman, 2016). Studies in a variety of insects, including locusts, dung beetles and monarch butterflies, have used intracellular recordings to chart maps of polarized light E-vectors in substructures of the region (Heinze and Homberg, 2007; el et al., 2015), and extracellular recordings from the cockroach have found sensory and motor correlates throughout the region (Bender et al., 2010; Guo and Ritzmann, 2012; Roy, 2012). More recently, calcium imaging experiments in behaving *Drosophila* have shown that both visual and motor cues can update a fly's internal representation of heading (Seelig and Jayaraman, 2015). Independently, neurogenetic studies have used disruptions of the normal physiology of the structure to highlight its involvement in a variety of functions, including motor coordination (Poeck et al., 2008), visual memory (Liu et al., 2006), sensory-motor adaptation (Triphan et al., 2010), and short- and long-term spatial memory (Neuser et al., 2008; Ofstad et al., 2011). It is likely that these tasks rely on the correct establishment and use of an internal representation of heading. Moreover, the scale of the network —a few thousands of neurons in the fly central complex— and the ease of genetic access to individual cell types in *Drosophila melanogaster*, make this circuit tractable with existing theoretical and experimental methods. Detailed light level anatomy (Hanesch et al., 1989; Wolff et al., 2015; Lin et al., 2013) of a significant fraction of the cell types, along with the availability of tools to genetically target these neurons by type (Wolff et al., 2015), have given rise to the first mechanistic

investigations of how the circuit constructs a stable heading representation (Kim et al., 2017), and how this representation updates as the animal turns in darkness (Turner-Evans et al., 2017; Green et al., 2017). Such results and related findings from other insects have also inspired a number of modeling studies aimed at predicting or reproducing physiologically and behaviorally relevant response patterns (Kakaria et al., 2017b; Givon et al., 2017; Chang et al., 2017; Cope et al., 2017; Su et al., 2017; Fiore et al., 2017; Kim et al., 2017; Stone et al., 2017; Turner-Evans et al., 2017). Many of these models make assumptions about connectivity within the central complex based on the degree of overlap at the light microscopy level between processes that look bouton-like and those that seem spiny, which are suggestive of pre- and post-synaptic specializations respectively. To go beyond those anatomical approaches, we constructed a connectivity map based on functional data, which includes information about whether connections are effectively excitatory or inhibitory. This map will help dissect the function of the central complex by constraining large-scale models and aiding the formulation and testing of new hypotheses. Given the likely number of existing and undiscovered cell types in the central complex, the diversity of neurotransmitters and receptors they express, the mixture of pre- and post-synaptic specializations in their arbors, and the dense recurrence of the network, we see this map as an initial scaffold, which will allow new information to be incorporated as it becomes available.

The quest to obtain circuit diagrams date back to Cajal and Golgi (y Cajal and Azoulay, 1894; Pannese, 1999), who used sparse labeling techniques to reveal neuron morphology and circuit architectures. Anatomical methods based on marking a discrete subset of neurons and imaging them with light microscopy have recently been revived in the form of techniques relying on stochastic genetic labeling (Livet et al., 2007; Hampel et al., 2011; Nern et al., 2015; Lee and Luo, 2001; Chiang et al., 2011) and photoactivatable fluorophores (Patterson, 2002; Ruta et al., 2010). These methods allow the extraction of the detailed anatomy of individual neurons. But even when used in combination with synaptic markers (Nicolai et al., 2010; DiAntonio et al., 1993; Zhang et al., 2002; Fouquet et al., 2009), such methods do not offer definitive evidence of synaptic connections, as they rely solely on the proximity of putative pre- and post-synaptic compartments. Recently, promising trans-synaptic genetic tagging systems (Talay et al., 2017; hao Huang et al., 2017) have been developed to address some of these issues. However, none of these approaches provide any insight into the functional properties of potential connections. Despite such shortcomings, light-level imaging constitutes a good starting point by constraining the search for possible connections within large populations of neurons —at the simplest level, if putative pre- and post-synaptic compartments do not overlap in light microscopy images, they cannot be in synaptic contact.

More recently, electron microscopy (EM) reconstruction has become the gold standard for connectomics (Briggman and Bock, 2012; Zheng et al., 2017; Schneider-Mizell et al., 2016). Under ideal conditions, it permits the unambiguous identification of synapses between all neurons in a given volume. As game-changing as this capability is, the technique also suffers from a few limitations. Acquiring, processing and analyzing the data is still time-consuming. As a result, connectomes from EM data are typically based on data from a single animal. In addition, EM does not permit the identification of neurotransmitter types at a given synapse, nor does it detect gap-junctions in invertebrate tissue, at least at present (Zheng et al., 2017). Finally, it can be challenging to assess the strengths of connections between two neurons, because it is not yet clear whether the number of synapses predicts the functional strength of the connection.

Functional methods address some of these drawbacks. Simple measures of activity have been used to assess a form of functional connectivity: regions or neurons whose simultaneously recorded activity is correlated —either spontaneously or during a given task— are deemed connected. This has been used with EEG, fMRI and MEG recordings in humans to establish maps at the brain region level (Salvador, 2004; Stam, 2004) and with multi-electrode recordings in monkeys and rodents (for example, Gerhard et al. 2011). Functional connectivity has also been inferred from correlations or graded changes in the response properties of neurons recorded in different animals, usually in cases where the neurons have overlapping arbors when examined with light microscopy. This approach has been employed to suggest polarized light processing pathways in

the central complex of the locust and monarch butterfly (Heinze et al., 2009; Heinze, 2014). However, such functional methods are correlative and do not provide a causal basis for the inferred connectivity.

To obtain a causal description of functional connectivity —sometimes termed effective connectivity— it is necessary to either stimulate one node of the network while recording from another one, or record both at sufficiently high resolution as to detect hallmarks of direct connectivity. The most reliable approach of this class is paired patch-clamp recording, which identifies connected pairs and their functional properties with a high level of detail (Huang et al., 2010; Yaksi and Wilson, 2010; Ω), but can only be performed at low throughput (Jiang et al., 2015). In recent years, the development of optogenetics has expanded the toolkit for simultaneous stimulation and recording experiments (Petreanu et al., 2007). In *Drosophila*, the ease of use of genetic reagents renders such approaches particularly attractive. Combinations of P2X2 and GCaMP (Yao et al., 2012), P2X2 and patch-clamp recordings (Hu et al., 2010), Channelrhodopsin-2 and patch-clamp (Gruntman and Turner, 2013) and CsChrimson and GCaMP (Hampel et al., 2015; Zhou et al., 2015; Ohyama et al., 2015) have been used in individual studies to investigate a small number of connections. Methods that rely on the genetic expression of calcium indicators to detect potential post-synaptic responses operate at a lower resolution than paired-recordings since they usually establish connectivity between cell types, as defined by the genetic driver lines used, rather than between individual neurons. These methods cannot definitively distinguish connections that are direct from those that might involve several synapses (but see Results/Discussion) and are limited by the sensitivity of the calcium sensors used. Despite these shortcomings, such methods constitute a good compromise as they still provide a causal measure of functional connectivity, and at a much higher throughput than double patch recordings. It is also worth noting that the advantages and limitations of these techniques complement those of serial EM reconstructions. We chose to apply this combination of optogenetics and calcium imaging on a large scale by systematically testing genetically defined pairs of central complex cell types, therefore building a large and extensible map of functional connections in the structure at cell-type resolution.

Cell types and hypothetical information flow in the central complex

The central complex consists of three main neuropiles — the protocerebral bridge (PB), the ellipsoid body (EB, Central Body Lower in other insects) and the fan-shaped body (FB, Central Body Upper in other insects) — and at least three accessory neuropiles — the noduli (NO), gall (GA) and lateral accessory lobe (LAL) (Figure S1A and Wolff et al. 2015; Lin et al. 2013; Hanesch et al. 1989). One of the most striking neural elements of the central complex are the *columnar neurons*, which innervate one of the eighteen (in Drosophila) glomeruli of the PB, one vertical section of either the FB or EB, and one accessory neuropile — a *column* being constituted by the PB glomeruli and FB/EB section. A total of 12 different columnar cell types have been described, with stereotypical correspondences between the PB glomerulus and the EB/FB section. In addition to these "principal cells", there are a number of neurons innervating multiple columns of one neuropile. These neurons often innervate subdivisions orthogonal to the columns. Moreover they sometimes also project to neuropiles outside the central complex . This set of neurons includes the ring neurons, which innervate a ring within the EB and an accessory neuropile, and a collection of inputs and interneurons with processes in the FB and PB. From this light level anatomy and putative synaptic polarity, one can derive a hypothetical general information flow diagram of the central complex (Figure S1Bi) :

- Ring neurons provide input to the EB columnar neurons.
- Recurrent connections between EB columnar neurons form and sustain a ring attractor for heading direction
- Information is transferred from the EB columnar system to the FB columnar system via the PB (interestingly, only one columnar neuron type displays presynaptic terminals in the PB, the E-PGs)
- FB columnar neurons also receive inputs in the FB
- All columnar neurons but the E-PGs also receive inputs in the PB

- Interneurons in the PB and FB further interconnect the columns
- All accessory structures are potential outputs

We show that this overall flow of information is generally supported functionally for the parts we have tested so far, but with a few potentially important differences (Figure S1Bii): the observed connectivity in the PB is sparse, rendering the function of PB interneurons possibly critical; accessory structures are usually input rather than output areas; and, consequently, output channels of the CX are scarce.

Results

A functional connectivity screen

We picked driver lines for functional connectivity mapping by visually inspecting the Janelia Gal4-driver collection (see Jenett et al., 2012) for strength of expression in the cell types of interest, and sparseness of the expression pattern in the central complex. The 37 driver lines (for 24 cell types) cover the main columnar neuron types and PB interneurons (Wolff et al., 2015), three types of ring neurons, a LAL-FB neuron and neurons innervating accessory structures, namely a LAL interneuron and three types of neurons connecting the LAL to the noduli. Neuron types are schematized in Figure S2A and Supplementary Figure S6. At the time of writing, the dataset includes inputs to the EB system, connections between EB columnar neurons, connections in the PB as well as potential inputs and outputs in the LAL, Gall and noduli. The connectivity of the multitude of cell types within the FB has not been explored.

Cell-type pairs to be tested were chosen based on overlaps between their expression patterns in light-level images. For each combination selected, we expressed CsChrimson and GCaMP6m in potential pre- and post-synaptic partners, respectively (Figure S2B,C), and probed their connection in an ex-vivo preparation using a standardized protocol (see Figure S2D, and Materials and Methods). Whenever large responses were observed, we used pharmacology to both check that observed transients were synaptically mediated, and to narrow down the neurotransmitters involved (Supplementary Figures S9 and S10).

Effects of stimulation ranged from very large and reliable transients (Figure S3Ai) to undetectable changes (Figure S3Aiii). In between those extremes, we observed transients of variable size and reliability (Figure S3B). To our surprise, we could also detect clear inhibitory responses (Figure S3Aii). It was possible because —at least in some cell types— fluctuations in baseline activity occasionally elevated GCaMP levels during the experiment (see Discussion and Supplementary Figure S11). Therefore, even though hyperpolarization below resting potential is likely not detectable through calcium imaging, we could detect inhibition from an excited state as a dip in the fluorescence trace.

Since no single characteristic of the responses could adequately capture their variety, variability and complexity, we chose to characterize the transients by using a battery of statistics reflecting response amplitude, shape, reliability and stimulus sensitivity (see Figure S3C, Supplementary Figure S8, and Materials and Methods). Responses of control pairs with non-overlapping processes were then used to form the null-hypothesis distributions of two metrics that capture response amplitude and reliability (see Figure S3D). For every data point, the Mahalanobis distance (see Methods) to the null distribution was computed and used as a connection strength metric in summary diagrams like Figure S4 and S5. Non-overlapping pairs usually showed no fluctuations upon stimulation, and when they did, they were small and unreliable (see

Supplementary Figure S7), likely reflecting indirect effects. Not surprisingly, responses were always detected with same-cell-type-stimulation controls (see Figure S3D).

All the individual responses and statistics, in the context of the overall connectivity diagram, are available at romainfr.github.io/CX-Functional-Website/, a website allowing the results of this screen to be explored interactively. We plan to update this website as further experiments are performed. The website can also be expanded to accommodate other sources of data, which would make it an exhaustive source of information about the central complex. The connectivity matrix resulting from our experiments is shown in Figure S4 in two alternative visualizations, namely a network diagram (Figure S4A) and a matrix of connection strengths (Figure S4B).

The central complex functional connectome

Figure S5 outlines some of the connectivity patterns we observed. We focus in particular on inputs and outputs relevant to parts of the central complex that we examined (the ellipsoid body, protocerebral bridge and paired noduli), connectivity within the protocerebral bridge, and components of the ring attractor network within the central complex.

Inputs

We identified two classes of inhibitory, picrotoxin-sensitive (hence mediated either by GABA-A or Glutamate) inputs to the central complex. First, the two ring neuron types we tested (GB-Eo, L-Ei) target the wedge columnar neurons (E-PG, Figure S5Ai), as has been suggested previously (Martín-Peña et al., 2014; Kahsai et al., 2012; Hanesch et al., 1989). Note that the ring neurons presented here are non-canonical : they do not innervate the bulb but either the LAL or the Gall. Second, a class of LAL-NO interneurons (the GL-N1 neuron) provides another source of inhibitory input into the EB columnar system by targeting the P-EN neurons (Figure S5Aii and S3Aii). This connection is particularly interesting in the light of the finding that the P-EN neurons drive the rotation of the bump of activity in the heading representation system (Green et al., 2017; Turner-Evans et al., 2017). Since the left/right noduli segregation corresponds to individual cells coding turns in opposite direction (Turner-Evans et al., 2017), the GL-N1 neurons are likely involved in strengthening or refining those turn related signals. Moreover, it is likely that other types of LAL-NO interneurons innervating other noduli compartments target P-FN neurons, but these pairs have not been tested extensively yet.

We also identified two excitatory inputs to the CX. First, a Gall to EB neuron, whose innervation pattern in the EB is reminiscent of the columnar neurons, excites the E-PG neurons (the same class that carries the heading representation and is inhibited by ring neurons). Second, several columnar neurons share excitatory inputs in the PB, from the IS-P neuron (PB.b-IB.s-SPS.s, Figure S5Aiii). It is important to note that although we tested very few candidates in the FB, it is highly likely that this region receives many inputs from outside the CX.

The neurons listed here do not necessarily provide feed-forward input from outside the CX. For example, the gall ring neuron (GB-Eo), which is an inhibitory input to the E-PGs, likely participates in a feedback loop, as it receives excitatory input from P-EG neurons (Figure S5Di). It is possible that this kind of loop between the columnar system and accessory structures input neurons is repeated in other places in the network.

Another example would be the IMPL-F neuron, which receives input from the PF-LCre neuron in the LAL. Its target in the CX has not been identified so far, but since it is located in the FB, it likely involves the FB columnar system.

Outputs

In contrast with inputs, we found few potential channels leaving the CX. The only output pathway identified in this dataset is presented in Figure S5C, and connects the PF-LCre columnar neuron to a LAL interneuron through a strong, mecamylamine-sensitive, excitatory connection (shown in figure S3Ai). This information is likely further processed in the LAL, as we found indications of inhibition upon PF-LCre stimulation in another LAL interneuron (WL-L). Even if we could not trace the circuit responsible for this inhibition, it likely involves an intermediate interneuron in the LAL. Once again, as this dataset does not include every single cell type of the CX, some outputs might easily have been missed. FB tangential neurons (Hanesch et al., 1989), for example, may also contribute output pathways.

Connectivity in the protocerebral bridge

A functional connectome is, by construction, sparser than can be predicted by light-level anatomy. Our study shows this most clearly in one neuropil, the PB (Figure S5B). E-PG neurons are the only columnar type that are presynaptic in the PB, but their activation did not trigger a significant response in any of the 5 other columnar neurons we tested. This came as a surprise as we assumed the E-PG population would constitute the relay between EB and FB columnar systems. To verify that this lack of observed connectivity was not due to the recruitment of global inhibitory circuits, we also ran these experiments in the presence of picrotoxin, and did not observe any difference in responses (see Supplementary Figure S10B). By contrast, the $\Delta 7$ interneurons are strongly activated by E-PG neurons, and their activation leads to significant responses in several columnar neuron types (E-PG, P-EN1, P-EN2, P-F1N3 and P-F3N2v). The $\Delta 7$ neurons, therefore, appear to constitute an important bottleneck in the system (Figure S5B), and may serve as the only strong link between columnar neurons in the PB. The response profiles following $\Delta 7$ activation are also unusually complex (see Supplementary Figure S13): P-ENs display mild activation, E-PG and P-F3N2v inhibition, and P-F1N3 strong rebound excitation (see Figure S3Biii).

Connectivity in the EB columnar system, the ring attractor network

Figure S5Dii shows the subpart of the network that has been proposed to sustain the ring attractor representation of heading (Green et al., 2017; Turner-Evans et al., 2017). One hypothesized feature of such a circuit is a large degree of recurrence between the different EB columnar types. In particular, P-EN to E-PG reciprocal connections are important for models of the rotation of the bump. While we found strong support for the P-EN1 to E-PG connection, the E-PG to P-EN1 connection that we reported functionally under a stronger stimulation protocol (Turner-Evans et al., 2017) may be mediated through the $\Delta 7$ interneurons. A few other connections were found in the EB (for example, P-EN1 to P-EN2), but it is important to stress that not all combinations could be tested due to limitations in the genetic reagents available. For example, the role of the P-EG neurons in this circuit, remains unclear. A key additional type that our results suggest may contribute in important ways to the persistence of activity in this circuit is the AMPG-E neuron, which appears to provide localized excitatory feedback to the E-PG neurons.

Discussion

The dataset presented in this study constitutes a resource for the growing community of researchers interested in the central complex. While similar coarse functional connectivity techniques have been used to map short pathways in previous studies, this is, to our knowledge, the first extensive dataset of its kind. We hope that it will become an evolving source of information, which we expect to be most useful when combined with other complementary data sources, such as EM-level anatomical connectivity and high-resolution gene expression profiles. Such combined data would constitute a solid base to build constrained network models of the central complex, and to generate detailed hypotheses of its function. As with any large dataset, we see this effort mainly as a starting point for more detailed research.

Limitations of the method

The connectivity technique we applied has several limitations that are important to keep in mind. First, the combination of CsChrimson and GCaMP does not guarantee that the connections observed are direct and monosynaptic. However, the large set of controls with cell-type pairs whose processes do not overlap provides a statistical framework to interpret the results — not surprisingly, uncertainty is highest for weak connections. A more pressing issue concerns sensitivity: what can be detected is limited by the stimulation protocol and the sensitivity of GCaMP6m. Thus, an absence of a post-synaptic response cannot be interpreted as an absence of a connection. The fact that inhibitory responses are visible, and that strong responses saturate with the range of stimulations used (see Supplementary Figure S12) is reassuring. It is likely, however, that EM-level anatomy will reveal that some weak synaptic connections have been missed by this technique. Their functional importance will need to be investigated using more sensitive methods, for example, intracellular electrophysiology. Further, we relied on full-field stimulation of populations of specific neuronal types, which comes with its own drawbacks: this approach provides no access to connectivity between neurons of the same class, and does not account for potential non-physiological network effects. One such effect would be the recruitment of global inhibitory networks that could mask an otherwise excitatory connection. However, whenever we suspected this could be a possibility, we controlled for it by blocking inhibition with picrotoxin, and never saw evidence of a significant effect (Supplementary Figure S10B). Even though picrotoxin was effective in blocking the inhibitory responses we observed (Supplementary Figure S10A), we cannot exclude the possibility that picrotoxin-insensitive inhibition (e.g. GABA-B, Olsen and Wilson 2008) might be present in the network. Furthermore, the fact that we stimulate whole presynaptic populations means that the strength of connections we report is influenced both by neuron-to-neuron transmission strength and the degree of convergence in the network. Finally, all our experiments were performed on ex-vivo brain preparations. Given the variety of neuromodulators that operate in the central complex (Kahsai et al., 2012), it is likely that functional connectivity within this region is modulated by brain state. Consistent with this possibility, we saw that the fluorescence baseline tended to fluctuate spontaneously during the course of our experiments in most types recorded (Supplementary Figure S11A). Although increases in baseline activity allowed us to detect inhibitory responses, we noticed that excitatory responses also occasionally depended on this baseline fluctuation (Supplementary Figure S11C).

Central complex motifs

The connectivity matrix we obtained is sparser than that predicted by light level anatomy. Our results suggest that the $\Delta 7$ interneurons are a bottleneck for information processing in the PB. This is all the more interesting given the range of responses evoked by $\Delta 7$ stimulation (Supplementary Figure S13). Properties of the synapses that $\Delta 7$ neurons make with their post-synaptic partners may play a primary role in the

way that a heading signal is generated and maintained in the EB columnar system, and also in how it may be transferred to the FB columnar system. Every $\Delta 7$ neuron innervates all columns of the PB, and has presynaptic-looking processes in two columns. The fact that a neuron with such extensive arbors participates in a circuit where representations are spatially restricted (the bump of activity is limited to a few neighboring columns) suggests that understanding local processing at the single neuron level might be critical to a complete understanding of how the circuit operates. Interestingly, the same puzzle occurs at the input side of the system with the ring neurons, which similarly innervate the entire circumference of the EB.

The fact that several sources of input are inhibitory raises the question of how activity is maintained in the region. Candidate mechanisms are the uncovered excitatory inputs into the PB and EB, recurrent connections in the EB and intrinsic properties of neurons (Egorov et al., 2002; Yoshida and Hasselmo, 2009; Russell and Hartline, 1982) — some cell types, for example, showed robust post-stimulation rebounds (see Figure S3Bii). It is also possible that our selection of cell types and our methods missed some sources of excitation.

The range of inputs revealed here opens many avenues for investigation. Whereas some ring neuron subtypes have received considerable attention (Sun et al., 2017; Shiozaki and Kazama, 2017; Seelig and Jayaraman, 2013), most PB inputs and LAL-noduli interneurons have not yet been characterized. A recent study in the sweat bee (Stone et al., 2017), for example, reported that one of the LAL-noduli interneurons — a likely input to the FB system — carries regressive optic flow signals.

The specific functions subserved by the network motifs that we have uncovered may only become clear with functional studies in behaving animals. A key puzzle set up by our findings is the small number of output channels of the central complex. Our results are consistent with the LAL being the primary output structure for the central complex (Chiang et al., 2011; Hanesch et al., 1989), although the structure also acts as an input region (via ring neurons and potentially via IMPF-L neurons). While it is possible that our selection of Gal4 lines was unintentionally biased against output neurons, or that our technique otherwise missed a number of output pathways, the picture of the central complex that emerges is of a densely recurrent sensorimotor hub with relatively low dimensional output (much as proposed by some models e.g. Stone et al. 2017; Fiore et al. 2015; Strauss and Berg 2010). The implications of this bottleneck for motor control remains a challenge for future studies to resolve.

Materials and methods

Fly stocks and crosses

For any given pair of neurons, drivers were chosen, and the overlap between pre- and post-synaptic looking regions assessed based on publicly available expression patterns (Tirian and Dickson 2017; Jenett et al. 2012, see Supplementary Figure S6) digitally aligned on a common reference brain (as described in Aso et al. 2014). For every LexA driver used, we prepared two stocks containing GCaMP6-m (Chen et al., 2013) and CsChrimson (Klapoetke et al., 2014) under LexAop (resp. UAS) or UAS (resp. LexAop) control : *XXX-LexA;13XLexAop2-IVS-p10-GCaMP6m 50.629 in VK00005, 20xUAS-CsChrimson-mCherry-trafficked in su(Hw)attP1* and *XXX-LexA;20xUAS-IVS-GCaMP6m 15.629 in attP2, 13XLexAop2-CsChrimson-tdTomato in VK00005*. Those stocks were then crossed to a Gal4 driver or a split-Gal4 (Luan et al., 2006) driver for the experiment. In the split-Gal4 case, the two split halves are inserted in attP40 and attP2 respectively. To avoid transvection between the split and the LexA driver (Mellert and Truman, 2012), we inserted the LexA drivers in alternative sites, either su(Hw)attP5 (Pfeiffer et al., 2010) or VK22 (Venken et al., 2006), and used the splits exclusively in combination with those lines after checking their expression

patterns. The list of drivers used and the corresponding cell types are given in Table 1. Throughout this paper we follow the naming convention set out in Wolff et al. 2015 for full names, and abbreviated following the scheme described in Kakaria et al. 2017a and used in Green et al. 2017 and Turner-Evans et al. 2017. For each cell type, we labeled every region innervated as pre- or post-synaptic (or both): this was done at the resolution of the glomerulus for the PB, the layer for the FB and the individual nodulus. We divided the LAL in three zones based on the overlap between the lines used. Existing subdivisions for the EB and Gall were preserved. This labeling was used to evaluate whether the arbors of a given cell-type-pair overlapped.

Dissections

The brains of 5 to 9 days old female flies were extracted and laid on a poly-D-lysine coated coverslip (Corning, Corning, NY). In most experiments, both the brain and the ventral nerve chord (VNC) were dissected out, as we found that having the VNC attached to the brain increased the mechanical stability of the preparation. Dissection was performed using the minimum level of illumination possible to avoid spurious activation of CsChrimson. The preparation was bathed throughout in saline containing (in mM): 103 NaCl, 3 KCl, 5 TES, 8 trehalose dihydrate, 10 glucose, 26 NaHCO$_3$, 1 NaH$_2$PO$_4$, 2 CaCl$_2$, 4 MgCl$_2$, bubbled with carbogen (95% O$_2$, 5% CO$_2$). Brains were positioned anterior-side-up, except when the connection tested was thought to be in the PB, in which case they were positioned posterior-side-up to maximize light access close to the assumed synaptic site. Trachea were removed. Only for experiments involving pharmacology, the glial sheath was gently torn with tweezers to enhance drug access to the neuropiles.

Imaging conditions and trial structure

Imaging was performed on an Ultima II 2-photon scanning microscope (Bruker, Billerica, MA) with a Vision II laser (Coherent, Santa Clara, CA). Brains were continuously perfused in the saline used for dissection at 60 mL/hour. Once the sample was placed and centered under the objective, we waited 5 minutes before starting the experiment to avoid any lingering network activation from the dissection or transmission lights. 2-photon excitation wavelength was 920 nm, and power at the sample varied between 3 and 10 mW. CsChrimson was excited with trains of 2 ms long 590 nm light pulses via an LED (M590L3-C1, Thorlabs, Newton, NJ) shone through the objective. The excitation light path contained a 605/55 bandpass filter and was delivered to the objective with a custom dichroic (zt488-568tpc, reflecting between 568nm and 700nm). On the detection arm, a 575nm dichroic beamsplitter and bandpass filters (525/70 nm and 607/45 nm for the green and red respectively) emitted photons to the PMTs (Hamamatsu multi-alkali). Instantaneous power measured out of the objective was roughly 50 µW/mm 2 . Stimulus pulse trains were delivered at 30 Hz and the number of pulses varied between 1,5,10, 20 and 30 — corresponding to total stimulation durations ranging from 2 ms to 1 s. Imaging fields of view were chosen as to avoid scanning regions containing CsChrimson-expressing neuropil while being as close as possible to the supposed connection site, as we observed occasional 2-photon stimulated slow activations of CsChrimson-expressing cells (high-intensity 2-photon stimulation of CsChrimson was used for spatially precise neuronal activation in Kim et al. 2017). When this was impossible — for example, in self-activation controls or for completely overlapping cell types — we chose a large ROI of which the CsChrimson/GCaMP6m-expressing neuropil represented a small fraction, so as to minimize duty cycle. ROIs were kept constant throughout the experiment. Each experimental run consisted of 4 repeats each approximately 16 s long. Runs were themselves repeated every 2 minutes. All experiments started with 5 runs corresponding to the five stimulation strengths, in a random order. This was sometimes followed by pharmacological testing. At the end of the experiment, a high intensity 3D stack was acquired to check that the expression patterns were as expected, and the correct region was imaged. At least 6 flies were tested for every pair considered.

Pharmacology

For blocking nicotinergic or inhibitory (GABAergic or glutamatergic) transmission, mecamylamine (50 µM) or picrotoxin (10 µM) (Sigma-Aldrich, St Louis, MO) were administered through the perfusion by switching to a different line for 3 minutes, followed by a wash period during which the perfusion was drug-free again. 30 pulses stimulations runs were repeated every 2 minutes, starting 4 minutes before the drug application and throughout the wash. Prior to use, they were kept frozen in 25 mM and 0.3 M aliquots, respectively.

Analysis

All analysis was performed in Julia, using custom-written routines. All data and code is available as an OpenScienceFramework project at `https://osf.io/vsa3z/`. Code is also centralized in this repository and notebooks recapitulating the analysis can be run straight from the browser here (using Binder).

Data processing

For a given experiment, all movies were aligned to each other to compensate for slow drifts of the sample: for each run, the average image was calculated, and translation drifts between average images were calculated using correlation-based sub-pixel registration (Guizar-Sicairos et al. 2008, and `https://github.com/romainFr/SubpixelRegistration.jl` for the Julia implementation used here). A region of interest (ROI) was defined for the full experiment: the average image (of all the runs) between foreground and background was distinguished using k-means clustering. Note that the selection method relies only on average intensity and not activity —a method we chose so as to maintain the same detection method for responsive and non-responsive runs. This also relies on selecting fields of view as unambiguously containing the neuron of interest — and only the neuron of interest — during the experiment.

$\Delta F/F_0 = \frac{(F - F_0)}{(F_0 - B)}$, where F is the raw fluorescence and B the background signal (calculated as the intensity of the 10% dimmest pixels of the average image) were then computed for each movie in the ROI. Given that baseline fluorescence could vary widely over the course of an experiment (see Discussion), we defined F_0 as the median fluorescence in the ROI in the dimmest 3% of frames of the entire experiment.

Statistics

For every experimental repeat, we computed the following statistics :

- F_{peak} the peak fluorescence value, and T_{peak} the time after stimulation at which the peak value is reached
- I_{toPeak} the integral of the signal up to the peak time
- $\tau_{1/2}$ the half-decay time
- F_{base} the fluorescence baseline before stimulation expressed in $\Delta F/F0$

Then, for every run, which consists of 4 repeats, we computed:

- $R_{within-flies}$ the average correlation between the 4 repeats of the run
- $<F_{peak}>$, $<T_{peak}>$, $<I_{toPeak}>$, $<F_{base}>$ and $<\tau_{1/2}>$ the medians of F_{peak}, T_{peak}, I_{toPeak}, F_{base} and $\tau_{1/2}$, respectively

Subsequently for every set of runs done on the same cell pair and the same stimulation protocol, we computed :

- $<<F_{peak}>>$, $<<T_{peak}>>$, $<<I_{toPeak}>>$, $<<F_{base}>>$, $<R_{repeats}>$ and $<<\tau_{1/2}>>$ the medians of $<F_{peak}>$, $<T_{peak}>$, $<I_{toPeak}>$, $<F_{base}>$, $R_{repeats}$ and $<\tau_{1/2}>$, respectively
- F_{peak_norm} and I_{toPeak_norm} the fluorescence peak and integral normalized to F_{base} (see Discussion)
- $R_{between\text{-}flies}$ the average correlation between the average responses of individual runs
- R_{state} the correlation between I_{toPeak} and F_{base}

Moreover we created $<I_{toPeak}>_{scaled}$ and $<<I_{toPeak}>>_{scaled}$, scaled versions of $<I_{toPeak}>$ and $<<I_{toPeak}>>$ so that the values cover the range [-1,1] by scaling positive (negative) values by the maximum (minimum) response in the dataset.

Distance from control and significance

Based on light level anatomy, we labeled each tested pair as overlapping or non-overlapping. We used the set of non overlapping pairs as a control (the null sample). Considering only two parameters, the scaled normalized integral and the correlation across flies (see Figure S3), we calculated the Mahalanobis distance between the null sample and each data point, using a robust estimate of the covariance matrix (Rousseeuw and Driessen, 1999) of the null sample. While single statistics never were sufficient to capture all relevant aspects of the response, we found that these two measurements recapitulated well distance measurements obtained by combining all the statistics. We then computed 99% confidence intervals on the distribution of distances by bootstrapping to determine significance.

Acknowledgments

Supplementary material

References

Yoshinori Aso, Daisuke Hattori, Yang Yu, Rebecca M Johnston, Nirmala A Iyer, Teri-TB Ngo, Heather Dionne, LF Abbott, Richard Axel, Hiromu Tanimoto, and Gerald M Rubin. The neuronal architecture of the mushroom body provides a logic for associative learning. *eLife*, 3, dec 2014. doi: 10.7554/elife.04577. URL https://doi.org/10.7554%2Felife.04577.

John A. Bender, Alan J. Pollack, and Roy E. Ritzmann. Neural Activity in the Central Complex of the Insect Brain Is Linked to Locomotor Changes. *Current Biology*, 20(10):921–926, may 2010. doi: 10.1016/j.cub.2010.03.054. URL https://doi.org/10.1016%2Fj.cub.2010.03.054.

Kevin L Briggman and Davi D Bock. Volume electron microscopy for neuronal circuit reconstruction. *Current Opinion in Neurobiology*, 22(1):154–161, feb 2012. doi: 10.1016/j.conb.2011.10.022. URL https://doi.org/10.1016%2Fj.conb.2011.10.022.

Po-Yen Chang, Ta-Shun Su, Chi-Tin Shih, and Chung-Chuan Lo. The Topographical Mapping in Drosophila Central Complex Network and Its Signal Routing. *Frontiers in Neuroinformatics*, 11, 2017. ISSN 1662-5196. doi: 10.3389/fninf.2017.00026. URL http://journal.frontiersin.org/article/10.3389/fninf.2017.00026/full.

Tsai-Wen Chen, Trevor J. Wardill, Yi Sun, Stefan R. Pulver, Sabine L. Renninger, Amy Baohan, Eric R. Schreiter, Rex A. Kerr, Michael B. Orger, Vivek Jayaraman, Loren L. Looger, Karel Svoboda, and Douglas S. Kim. Ultrasensitive fluorescent proteins for imaging neuronal activity. *Nature*, 499(7458):295–300, jul 2013. ISSN 0028-0836. doi: 10.1038/nature12354. URL http://www.nature.com/nature/journal/v499/n7458/abs/nature12354.html.

Ann-Shyn Chiang, Chih-Yung Lin, Chao-Chun Chuang, Hsiu-Ming Chang, Chang-Huain Hsieh, Chang-Wei Yeh, Chi-Tin Shih, Jian-Jheng Wu, Guo-Tzau Wang, Yung-Chang Chen, Cheng-Chi Wu, Guan-Yu Chen, Yu-Tai Ching, Ping-Chang Lee, Chih-Yang Lin, Hui-Hao Lin, Chia-Chou Wu, Hao-Wei Hsu, Yun-Ann Huang, Jing-Yi Chen, Hsin-Jung Chiang, Chun-Fang Lu, Ru-Fen Ni, Chao-Yuan Yeh, and Jenn-Kang Hwang. Three-Dimensional Reconstruction of Brain-wide Wiring Networks in Drosophila at Single-Cell Resolution. *Current Biology*, 21(1):1–11, jan 2011. doi: 10.1016/j.cub.2010.11.056. URL https://doi.org/10.1016%2Fj.cub.2010.11.056.

Alex J. Cope, Chelsea Sabo, Eleni Vasilaki, Andrew B. Barron, and James A. R. Marshall. A computational model of the integration of landmarks and motion in the insect central complex. *PLOS ONE*, 12(2): e0172325, feb 2017. doi: 10.1371/journal.pone.0172325. URL https://doi.org/10.1371%2Fjournal.pone.0172325.

A DiAntonio, RW Burgess, AC Chin, DL Deitcher, RH Scheller, and TL Schwarz. Identification and characterization of Drosophila genes for synaptic vesicle proteins. *J Neurosci*, 13:4924–35, Nov 1993.

AV Egorov, BN Hamam, E Fransén, ME Hasselmo, and AA Alonso. Graded persistent activity in entorhinal cortex neurons. *Nature*, 420:173–8, Nov 2002.

Jundi B el, EJ Warrant, MJ Byrne, L Khaldy, E Baird, J Smolka, and M Dacke. Neural coding underlying the cue preference for celestial orientation. *Proc Natl Acad Sci U S A*, 112:11395–400, Sep 2015.

VG Fiore, RJ Dolan, NJ Strausfeld, and F Hirth. Evolutionarily conserved mechanisms for the selection and maintenance of behavioural activity. *Philos Trans R Soc Lond B Biol Sci*, 370, Dec 2015.

Vincenzo G. Fiore, Benjamin Kottler, Xiaosi Gu, and Frank Hirth. In silico Interrogation of Insect Central Complex Suggests Computational Roles for the Ellipsoid Body in Spatial Navigation. *Frontiers in Behavioral Neuroscience*, 11, aug 2017. doi: 10.3389/fnbeh.2017.00142. URL https://doi.org/10.3389%2Ffnbeh.2017.00142.

Wernher Fouquet, David Owald, Carolin Wichmann, Sara Mertel, Harald Depner, Marcus Dyba, Stefan Hallermann, Robert J. Kittel, Stefan Eimer, and Stephan J. Sigrist. Maturation of active zone assembly by-DrosophilaBruchpilot. *The Journal of Cell Biology*, 186(1):129–145, jul 2009. doi: 10.1083/jcb.200812150. URL https://doi.org/10.1083%2Fjcb.200812150.

Felipe Gerhard, Gordon Pipa, Bruss Lima, Sergio Neuenschwander, and Wulfram Gerstner. Extraction of Network Topology From Multi-Electrode Recordings: Is there a Small-World Effect? *Frontiers in Computational Neuroscience*, 5, 2011. doi: 10.3389/fncom.2011.00004. URL https://doi.org/10.3389%2Ffncom.2011.00004.

Lev E. Givon, Aurel A. Lazar, and Chung-Heng Yeh. Generating Executable Models of the Drosophila Central Complex. *Frontiers in Behavioral Neuroscience*, 11:102, 2017. doi: 10.3389/fnbeh.2017.00102.

Jonathan Green, Atsuko Adachi, Kunal K. Shah, Jonathan D. Hirokawa, Pablo S. Magani, and Gaby Maimon. A neural circuit architecture for angular integration in Drosophila. *Nature*, 546(7656):101–106, may 2017. doi: 10.1038/nature22343. URL https://doi.org/10.1038%2Fnature22343.

Eyal Gruntman and Glenn C. Turner. Integration of the olfactory code across dendritic claws of single mushroom body neurons. *Nature Neuroscience*, 16(12):1821–1829, dec 2013. ISSN 1546-1726. doi: 10.1038/nn.3547.

Manuel Guizar-Sicairos, Samuel T. Thurman, and James R. Fienup. Efficient subpixel image registration algorithms. *Optics Letters*, 33(2):156–158, jan 2008. ISSN 1539-4794. doi: 10.1364/OL.33.000156. URL http://www.osapublishing.org/abstract.cfm?uri=ol-33-2-156.

P. Guo and R. E. Ritzmann. Neural activity in the central complex of the cockroach brain is linked to turning behaviors. *Journal of Experimental Biology*, 216(6):992–1002, nov 2012. doi: 10.1242/jeb.080473. URL https://doi.org/10.1242%2Fjeb.080473.

Stefanie Hampel, Phuong Chung, Claire E McKellar, Donald Hall, Loren L Looger, and Julie H Simpson. Drosophila Brainbow: a recombinase-based fluorescence labeling technique to subdivide neural expression patterns. *Nature Methods*, 8(3):253–259, feb 2011. doi: 10.1038/nmeth.1566. URL https://doi.org/10.1038%2Fnmeth.1566.

U. Hanesch, K. F. Fischbach, and M. Heisenberg. Neuronal architecture of the central complex in Drosophila melanogaster. *Cell and Tissue Research*, 257(2):343–366, 1989. doi: 10.1007/bf00261838. URL https://doi.org/10.1007%2Fbf00261838.

Ting hao Huang, Peter Niesman, Deepshika Arasu, Daniel Lee, Aubrie De La Cruz, Antuca Callejas, Elizabeth J Hong, and Carlos Lois. Tracing neuronal circuits in transgenic animals by transneuronal control of transcription (TRACT). *eLife*, 6, dec 2017. doi: 10.7554/elife.32027. URL https://doi.org/10.7554%2Felife.32027.

S. Heinze and U. Homberg. Maplike Representation of Celestial E-Vector Orientations in the Brain of an Insect. *Science*, 315(5814):995–997, feb 2007. doi: 10.1126/science.1135531. URL https://doi.org/10.1126%2Fscience.1135531.

S. Heinze, S. Gotthardt, and U. Homberg. Transformation of Polarized Light Information in the Central Complex of the Locust. *Journal of Neuroscience*, 29(38):11783–11793, sep 2009. doi: 10.1523/jneurosci.1870-09.2009. URL https://doi.org/10.1523%2Fjneurosci.1870-09.2009.

Stanley Heinze. Polarized-Light Processing in Insect Brains: Recent Insights from the Desert Locust the Monarch Butterfly, the Cricket, and the Fruit Fly. In *Polarized Light and Polarization Vision in Animal Sciences*, pages 61–111. Springer Berlin Heidelberg, 2014. doi: 10.1007/978-3-642-54718-8_4. URL https://doi.org/10.1007%2F978-3-642-54718-8_4.

Aiqun Hu, Wei Zhang, and Zuoren Wang. Functional feedback from mushroom bodies to antennal lobes in the Drosophila olfactory pathway. *Proceedings of the National Academy of Sciences*, 107(22):10262–10267, jun 2010. ISSN 0027-8424, 1091-6490. doi: 10.1073/pnas.0914912107. URL http://www.pnas.org/content/107/22/10262.

Ju Huang, Wei Zhang, Wenhui Qiao, Aiqun Hu, and Zuoren Wang. Functional Connectivity and Selective Odor Responses of Excitatory Local Interneurons in Drosophila Antennal Lobe. *Neuron*, 67(6):1021–1033, sep 2010. doi: 10.1016/j.neuron.2010.08.025. URL https://doi.org/10.1016%2Fj.neuron.2010.08.025.

Arnim Jenett, Gerald M. Rubin, Teri-T.B. Ngo, David Shepherd, Christine Murphy, Heather Dionne, Barret D. Pfeiffer, Amanda Cavallaro, Donald Hall, Jennifer Jeter, Nirmala Iyer, Dona Fetter, Joanna H. Hausenfluck, Hanchuan Peng, Eric T. Trautman, Robert R. Svirskas, Eugene W. Myers, Zbigniew R. Iwinski, Yoshinori Aso, Gina M. DePasquale, Adrianne Enos, Phuson Hulamm, Shing Chun Benny Lam, Hsing-Hsi Li, Todd R. Laverty, Fuhui Long, Lei Qu, Sean D. Murphy, Konrad Rokicki, Todd Safford, Kshiti Shaw, Julie H. Simpson, Allison Sowell, Susana Tae, Yang Yu, and Christopher T. Zugates. A GAL4-Driver Line Resource for Drosophila Neurobiology. *Cell Reports*, 2(4):991–1001, oct 2012. doi: 10.1016/j.celrep.2012.09.011. URL https://doi.org/10.1016%2Fj.celrep.2012.09.011.

X. Jiang, S. Shen, C. R. Cadwell, P. Berens, F. Sinz, A. S. Ecker, S. Patel, and A. S. Tolias. Principles of connectivity among morphologically defined cell types in adult neocortex. *Science*, 350(6264):aac9462–aac9462, nov 2015. doi: 10.1126/science.aac9462. URL https://doi.org/10.1126%2Fscience.aac9462.

L. Kahsai, M.A. Carlsson, Å.M.E. Winther, and D.R. Nässel. Distribution of metabotropic receptors of serotonin dopamine, GABA glutamate, and short neuropeptide F in the central complex of Drosophila. *Neuroscience*, 208:11–26, apr 2012. doi: 10.1016/j.neuroscience.2012.02.007. URL https://doi.org/10.1016%2Fj.neuroscience.2012.02.007.

Kyobi S. Kakaria, De Bivort, and Benjamin L. Ring Attractor Dynamics Emerge from a Spiking Model of the Entire Protocerebral Bridge. *Frontiers in Behavioral Neuroscience*, 11, 2017a. ISSN 1662-5153. doi: 10.3389/fnbeh.2017.00008. URL http://journal.frontiersin.org/article/10.3389/fnbeh.2017.00008/abstract.

Kyobi S. Kakaria, De Bivort, and Benjamin L. Ring Attractor Dynamics Emerge from a Spiking Model of the Entire Protocerebral Bridge. *Frontiers in Behavioral Neuroscience*, 11, 2017b. ISSN 1662-5153. doi: 10.3389/fnbeh.2017.00008. URL http://journal.frontiersin.org/article/10.3389/fnbeh.2017.00008/abstract.

Sung Soo Kim, Hervé Rouault, Shaul Druckmann, and Vivek Jayaraman. Ring attractor dynamics in the Drosophila central brain. *Science*, 356(6340):849–853, may 2017. doi: 10.1126/science.aal4835. URL https://doi.org/10.1126%2Fscience.aal4835.

Nathan C Klapoetke, Yasunobu Murata, Sung Soo Kim, Stefan R Pulver, Amanda Birdsey-Benson, Yong Ku Cho, Tania K Morimoto, Amy S Chuong, Eric J Carpenter, Zhijian Tian, Jun Wang, Yinlong Xie, Zhixiang Yan, Yong Zhang, Brian Y Chow, Barbara Surek, Michael Melkonian, Vivek Jayaraman, Martha Constantine-Paton, Gane Ka-Shu Wong, and Edward S Boyden. Independent optical excitation of distinct neural populations. *Nature Methods*, 11(3):338–346, feb 2014. ISSN 1548-7091, 1548-7105. doi: 10.1038/nmeth.2836. URL http://www.nature.com/doifinder/10.1038/nmeth.2836.

Tzumin Lee and Liqun Luo. Mosaic analysis with a repressible cell marker (MARCM) for Drosophila neural development. *Trends in Neurosciences*, 24(5):251–254, may 2001. doi: 10.1016/s0166-2236(00)01791-4. URL https://doi.org/10.1016%2Fs0166-2236%2800%2901791-4.

Chih-Yung Lin, Chao-Chun Chuang, Tzu-En Hua, Chun-Chao Chen, Barry J. Dickson, Ralph J. Greenspan, and Ann-Shyn Chiang. A Comprehensive Wiring Diagram of the Protocerebral Bridge for Visual Information Processing in the Drosophila Brain. *Cell Reports*, 3(5):1739–1753, may 2013. doi: 10.1016/j.celrep.2013.04.022. URL https://doi.org/10.1016%2Fj.celrep.2013.04.022.

G Liu, H Seiler, A Wen, T Zars, K Ito, R Wolf, M Heisenberg, and L Liu. Distinct memory traces for two visual features in the Drosophila brain. *Nature*, 439:551–6, Feb 2006.

Jean Livet, Tamily A. Weissman, Hyuno Kang, Ryan W. Draft, Ju Lu, Robyn A. Bennis, Joshua R. Sanes, and Jeff W. Lichtman. Transgenic strategies for combinatorial expression of fluorescent proteins in the nervous system. *Nature*, 450(7166):56–62, nov 2007. doi: 10.1038/nature06293. URL https://doi.org/10.1038%2Fnature06293.

Haojiang Luan, Nathan C. Peabody, Charles R. Vinson, and Benjamin H. White. Refined Spatial Manipulation of Neuronal Function by Combinatorial Restriction of Transgene Expression. *Neuron*, 52(3):425–436, nov 2006. ISSN 08966273. doi: 10.1016/j.neuron.2006.08.028. URL http://linkinghub.elsevier.com/retrieve/pii/S089662730600674X.

Alfonso Martín-Peña, Angel Acebes, José-Rodrigo Rodríguez, Valerie Chevalier, Sergio Casas-Tinto, Tilman Triphan, Roland Strauss, and Alberto Ferrús. Cell types and coincident synapses in the ellipsoid body ofDrosophila. *European Journal of Neuroscience*, 39(10):1586–1601, mar 2014. doi: 10.1111/ejn.12537. URL https://doi.org/10.1111%2Fejn.12537.

David J. Mellert and James W. Truman. Transvection Is Common Throughout the Drosophila Genome. *Genetics*, 191(4):1129–1141, aug 2012. ISSN 0016-6731, 1943-2631. doi: 10.1534/genetics.112.140475. URL http://www.genetics.org/content/191/4/1129.

Aljoscha Nern, Barret D. Pfeiffer, and Gerald M. Rubin. Optimized tools for multicolor stochastic labeling reveal diverse stereotyped cell arrangements in the fly visual system. *Proceedings of the National Academy of Sciences*, 112(22):E2967–E2976, may 2015. doi: 10.1073/pnas.1506763112. URL https://doi.org/10.1073%2Fpnas.1506763112.

Kirsa Neuser, Tilman Triphan, Markus Mronz, Burkhard Poeck, and Roland Strauss. Analysis of a spatial orientation memory in Drosophila. *Nature*, 453(7199):1244–1247, may 2008. doi: 10.1038/nature07003. URL https://doi.org/10.1038%2Fnature07003.

L. J. J. Nicolai, A. Ramaekers, T. Raemaekers, A. Drozdzecki, A. S. Mauss, J. Yan, M. Landgraf, W. Annaert, and B. A. Hassan. Genetically encoded dendritic marker sheds light on neuronal connectivity in Drosophila. *Proceedings of the National Academy of Sciences*, 107(47):20553–20558, nov 2010. doi: 10.1073/pnas.1010198107. URL https://doi.org/10.1073%2Fpnas.1010198107.

Tyler A. Ofstad, Charles S. Zuker, and Michael B. Reiser. Visual place learning in Drosophila melanogaster. *Nature*, 474(7350):204–207, jun 2011. doi: 10.1038/nature10131. URL https://doi.org/10.1038%2Fnature10131.

Shawn R. Olsen and Rachel I. Wilson. Lateral presynaptic inhibition mediates gain control in an olfactory circuit. *Nature*, 452(7190):956–960, mar 2008. doi: 10.1038/nature06864. URL https://doi.org/10.1038%2Fnature06864.

Ennio Pannese. The Golgi Stain: Invention Diffusion and Impact on Neurosciences. *Journal of the History of the Neurosciences*, 8(2):132–140, aug 1999. doi: 10.1076/jhin.8.2.132.1847. URL https://doi.org/10.1076%2Fjhin.8.2.132.1847.

G. H. Patterson. A Photoactivatable GFP for Selective Photolabeling of Proteins and Cells. *Science*, 297 (5588):1873–1877, sep 2002. doi: 10.1126/science.1074952. URL https://doi.org/10.1126%2Fscience.1074952.

L Petreanu, D Huber, A Sobczyk, and K Svoboda. Channelrhodopsin-2-assisted circuit mapping of long-range callosal projections. *Nat Neurosci*, 10:663–8, May 2007.

Barret D. Pfeiffer, Teri-T. B. Ngo, Karen L. Hibbard, Christine Murphy, Arnim Jenett, James W. Truman, and Gerald M. Rubin. Refinement of Tools for Targeted Gene Expression in Drosophila. *Genetics*, 186(2):735–755, oct 2010. ISSN 0016-6731, 1943-2631. doi: 10.1534/genetics.110.119917. URL http://www.genetics.org/content/186/2/735.

Burkhard Poeck, Tilman Triphan, Kirsa Neuser, and Roland Strauss. Locomotor control by the central complex inDrosophila—An analysis of thetay bridge mutant. *Developmental Neurobiology*, 68(8):1046–1058, 2008. doi: 10.1002/dneu.20643. URL https://doi.org/10.1002%2Fdneu.20643.

Peter J. Rousseeuw and Katrien Van Driessen. A Fast Algorithm for the Minimum Covariance Determinant Estimator. *Technometrics*, 41(3):212–223, aug 1999. doi: 10.1080/00401706.1999.10485670. URL https://doi.org/10.1080%2F00401706.1999.10485670.

Ritzmann Roy. Encoding Sensory Information in the Central Complex of the Cockroach. *Frontiers in Behavioral Neuroscience*, 6, 2012. doi: 10.3389/conf.fnbeh.2012.27.00313. URL https://doi.org/10.3389%2Fconf.fnbeh.2012.27.00313.

DF Russell and DK Hartline. Slow active potentials and bursting motor patterns in pyloric network of the lobster, Panulirus interruptus. *J Neurophysiol*, 48:914–37, Oct 1982.

Vanessa Ruta, Sandeep Robert Datta, Maria Luisa Vasconcelos, Jessica Freeland, Loren L. Looger, and Richard Axel. A dimorphic pheromone circuit in Drosophila from sensory input to descending output. *Nature*, 468(7324):686–690, dec 2010. doi: 10.1038/nature09554. URL https://doi.org/10.1038%2Fnature09554.

R. Salvador. Neurophysiological Architecture of Functional Magnetic Resonance Images of Human Brain. *Cerebral Cortex*, 15(9):1332–1342, dec 2004. doi: 10.1093/cercor/bhi016. URL https://doi.org/10.1093%2Fcercor%2Fbhi016.

Casey M Schneider-Mizell, Stephan Gerhard, Mark Longair, Tom Kazimiers, Feng Li, Maarten F Zwart, Andrew Champion, Frank M Midgley, Richard D Fetter, Stephan Saalfeld, and Albert Cardona. Quantitative neuroanatomy for connectomics in Drosophila. *eLife*, 5, mar 2016. doi: 10.7554/elife.12059. URL https://doi.org/10.7554%2Felife.12059.

JD Seelig and V Jayaraman. Feature detection and orientation tuning in the Drosophila central complex. *Nature*, 503:262–6, Nov 2013.

Johannes D. Seelig and Vivek Jayaraman. Neural dynamics for landmark orientation and angular path integration. *Nature*, 521(7551):186–191, may 2015. doi: 10.1038/nature14446. URL https://doi.org/10.1038%2Fnature14446.

Hiroshi M Shiozaki and Hokto Kazama. Parallel encoding of recent visual experience and self-motion during navigation in Drosophila. *Nature Neuroscience*, 20(10):1395–1403, sep 2017. doi: 10.1038/nn.4628. URL https://doi.org/10.1038%2Fnn.4628.

C.J. Stam. Functional connectivity patterns of human magnetoencephalographic recordings: a 'small-world' network? *Neuroscience Letters*, 355(1-2):25–28, jan 2004. doi: 10.1016/j.neulet.2003.10.063. URL https://doi.org/10.1016%2Fj.neulet.2003.10.063.

T Stone, B Webb, A Adden, NB Weddig, A Honkanen, R Templin, W Wcislo, L Scimeca, E Warrant, and S Heinze. An Anatomically Constrained Model for Path Integration in the Bee Brain. *Curr Biol*, 27: 3069–3085.e11, Oct 2017.

Roland Strauss and Christian Berg. The central control of oriented locomotion in insects - towards a neurobiological model. In *The 2010 International Joint Conference on Neural Networks (IJCNN)*. IEEE, jul 2010. doi: 10.1109/ijcnn.2010.5596461. URL https://doi.org/10.1109%2Fijcnn.2010.5596461.

Ta-Shun Su, Wan-Ju Lee, Yu-Chi Huang, Cheng-Te Wang, and Chung-Chuan Lo. Coupled symmetric and asymmetric circuits underlying spatial orientation in fruit flies. *Nature Communications*, 8(1), jul 2017. doi: 10.1038/s41467-017-00191-6. URL https://doi.org/10.1038%2Fs41467-017-00191-6.

Yi Sun, Aljoscha Nern, Romain Franconville, Hod Dana, Eric R Schreiter, Loren L Looger, Karel Svoboda, Douglas S Kim, Ann M Hermundstad, and Vivek Jayaraman. Neural signatures of dynamic stimulus selection in Drosophila. *Nature Neuroscience*, 20(8):1104–1113, jun 2017. doi: 10.1038/nn.4581. URL https://doi.org/10.1038%2Fnn.4581.

Mustafa Talay, Ethan B. Richman, Nathaniel J. Snell, Griffin G. Hartmann, John D. Fisher, Altar Sorkaç, Juan F. Santoyo, Cambria Chou-Freed, Nived Nair, Mark Johnson, John R. Szymanski, and Gilad Barnea. Transsynaptic Mapping of Second-Order Taste Neurons in Flies by trans -Tango. *Neuron*, 96(4):783–795.e4, nov 2017. doi: 10.1016/j.neuron.2017.10.011. URL https://doi.org/10.1016%2Fj.neuron.2017.10.011.

Laszlo Tirian and Barry Dickson. The VT GAL4 LexA and split-GAL4 driver line collections for targeted expression in the Drosophila nervous system. oct 2017. doi: 10.1101/198648. URL https://doi.org/10.1101%2F198648.

Tilman Triphan, Burkhard Poeck, Kirsa Neuser, and Roland Strauss. Visual Targeting of Motor Actions

in Climbing Drosophila. *Current Biology*, 20(7):663–668, apr 2010. doi: 10.1016/j.cub.2010.02.055. URL https://doi.org/10.1016%2Fj.cub.2010.02.055.

Daniel Turner-Evans, Stephanie Wegener, Hervé Rouault, Romain Franconville, Tanya Wolff, Johannes D Seelig, Shaul Druckmann, and Vivek Jayaraman. Angular velocity integration in a fly heading circuit. *eLife*, 6, may 2017. doi: 10.7554/elife.23496. URL https://doi.org/10.7554%2Felife.23496.

DB Turner-Evans and V Jayaraman. The insect central complex. *Curr Biol*, 26:R453–7, Jun 2016.

Koen J. T. Venken, Yuchun He, Roger A. Hoskins, and Hugo J. Bellen. P[acman]: A BAC Transgenic Platform for Targeted Insertion of Large DNA Fragments in D. melanogaster. *Science*, 314(5806):1747–1751, dec 2006. ISSN 0036-8075, 1095-9203. doi: 10.1126/science.1134426. URL http://science.sciencemag.org/content/314/5806/1747.

Tanya Wolff, Nirmala A. Iyer, and Gerald M. Rubin. Neuroarchitecture and neuroanatomy of the *Drosophila* central complex: A GAL4-based dissection of protocerebral bridge neurons and circuits: *Drosophila* Central Complex Anatomy and Neurons. *Journal of Comparative Neurology*, 523(7):997–1037, may 2015. ISSN 00219967. doi: 10.1002/cne.23705. URL http://doi.wiley.com/10.1002/cne.23705.

Santiago Ramón y Cajal and L. Azoulay. *Les nouvelles idées sur la structure du système nerveux : chez l'homme et chez les vertébrés /*. C. Reinwald & Cie.,, 1894. doi: 10.5962/bhl.title.48561. URL https://doi.org/10.5962%2Fbhl.title.48561.

E Yaksi and RI Wilson. Electrical coupling between olfactory glomeruli. *Neuron*, 67:1034–47, Sep 2010.

Zepeng Yao, Ann Marie Macara, Katherine R. Lelito, Tamara Y. Minosyan, and Orie T. Shafer. Analysis of functional neuronal connectivity in the Drosophila brain. *Journal of Neurophysiology*, 108(2):684–696, jul 2012. ISSN 1522-1598. doi: 10.1152/jn.00110.2012.

M Yoshida and ME Hasselmo. Persistent firing supported by an intrinsic cellular mechanism in a component of the head direction system. *J Neurosci*, 29:4945–52, Apr 2009.

Yong Q. Zhang, Christopher K. Rodesch, and Kendal Broadie. Living synaptic vesicle marker: Synaptotagmin-GFP. *genesis*, 34(1-2):142–145, sep 2002. doi: 10.1002/gene.10144. URL https://doi.org/10.1002%2Fgene.10144.

Zhihao Zheng, J. Scott Lauritzen, Eric Perlman, Camenzind G. Robinson, Matthew Nichols, Daniel Milkie, Omar Torrens, John Price, Corey B. Fisher, Nadiya Sharifi, Steven A. Calle-Schuler, Lucia Kmecova, Iqbal J. Ali, Bill Karsh, Eric T. Trautman, John Bogovic, Philipp Hanslovsky, Gregory S. X. E. Jefferis, Michael Kazhdan, Khaled Khairy, Stephan Saalfeld, Richard D. Fetter, and Davi D. Bock. A Complete Electron Microscopy Volume Of The Brain Of Adult Drosophila melanogaster. may 2017. doi: 10.1101/140905. URL https://doi.org/10.1101%2F140905.

Line	Wolff Type Name	New Type Name	Type Description	Supertype
87G07	4	P-F3N2d	PBG2-9.s-FBl3.b-NO2D.b	FB columnar
85H06	1-2	P-F1N3	PBG2-9.s-FBl1.b-NO3PM.b	FB columnar
60D05	8	E-PG	PBG1-8.b-EBw.s-DV_GA.b	EB columnar
SS02191	7	P-EG	PBG1-8.s-EBt.b-DV_GA.b	EB columnar
67D09	5	P-F3N2v	PBG2-9.s-FBl3.b-NO2V.b	FB columnar
67D09-attP5	5	P-F3N2v	PBG2-9.s-FBl3.b-NO2V.b	FB columnar
67D09-VK22	5	P-F3N2v	PBG2-9.s-FBl3.b-NO2V.b	FB columnar
37F06	6	P-EN1	PBG2-9.s-EBt.b-NO1.b.Type1	EB columnar
37F06-VK22	6	P-EN1	PBG2-9.s-EBt.b-NO1.b.Type1	EB columnar
VT008135	6	P-EN1	PBG2-9.s-EBt.b-NO1.b.Type1	EB columnar
SS02232	6	P-EN2	PBG2-9.s-EBt.b-NO1.b.Type2	EB columnar
84H05	12	PF-LCre	PBG1-7.s-FBl2.s-LAL.b-cre.b	FB columnar
84H05-VK22	12	PF-LCre	PBG1-7.s-FBl2.s-LAL.b-cre.b	FB columnar
84H05-attP5	12	PF-LCre	PBG1-7.s-FBl2.s-LAL.b-cre.b	FB columnar
55G08	15	Delta7	PB18.s-GxΔ7Gy.b-PB18.s-9i1i8c.b	PB interneuron
55G08-attP5	15	Delta7	PB18.s-GxΔ7Gy.b-PB18.s-9i1i8c.b	PB interneuron
55G08-VK22	15	Delta7	PB18.s-GxΔ7Gy.b-PB18.s-9i1i8c.b	PB interneuron
47G08	17	IS-P	PBG2-9.b-IB.s.SPS.s	PB input
49H05		IMPL-F	LAL.s-IMP-FBl3.b	FB input
75H04		L-Ei	EBIRP I-O-LAL.s	Ring neuron
32A11		L-Em	EBMRP I-O-LAL.s	Ring neuron
18A05		GB-Eo	EBORP O-I-GA-Bulb	Ring neuron
18A05-VK22		GB-Eo	EBORP O-I-GA-Bulb	Ring neuron
17H12		AMPG-E	EB.w-AMP.d-D_GAsurround	EB input
12C11		EFBG	EBMRA-FB-LT-LT-GA-GA	Other
72H06		SMPL-L	SMP.s-LAL.s-LAL.b.contra	LAL-IN
72H06-attP5		SMPL-L	SMP.s-LAL.s-LAL.b.contra	LAL-IN
72H06-VK22		SMPL-L	SMP.s-LAL.s-LAL.b.contra	LAL-IN
SS02615		SMPL-L2	SMP.s-LAL.s-LAL.b.contra2	LAL-IN
26B07		WL-L	Wedge-LAL.s-LAL.b.contra	LAL-IN
31A11		L-Cre	LAL-Cre	LAL-IN
SS00153		S-P	SPS.s-PB.b	PB input
76E11		GL-N1	LAL.s-GAi.s-NO1i.b	LAL-NO
76E11-VK22		GL-N1	LAL.s-GAi.s-NO1i.b	LAL-NO
SS04448		GL-N1	LAL.s-GAi.s-NO1i.b	LAL-NO
SS04420		CreL-N2	Cre.s-LAL.s-NO2.b	LAL-NO
12G04		L-N3	LAL.s-NO3Ai.b	LAL-NO

Table 1: Drivers and neuron types used. "Wolff Type Name" refers to the type names as described in (Wolff et al., 2015), "New Type Name" to the nomenclature for short names adopted in this paper (following Kakaria et al. 2017a; Turner-Evans et al. 2017; Green et al. 2017). Type description is the long name, following the guidelines of (Wolff et al., 2015). Pre and post regions are labeled based on anatomical characteristics. The fine subdivisions were used to establish if two neurons are anatomically overlapping.

Figure S1: The central complex neuropiles and the hypothesized flow of information based on overlap of arbors in light-microscopy images. A: Schematic representation of the central complex and associated structures used throughout the manuscript. B: (i) Hypothesized global information flow in the central complex based on neuron morphologies and the overlap of processes between different neuron types. (ii) Connectivity map based on the results of this study.
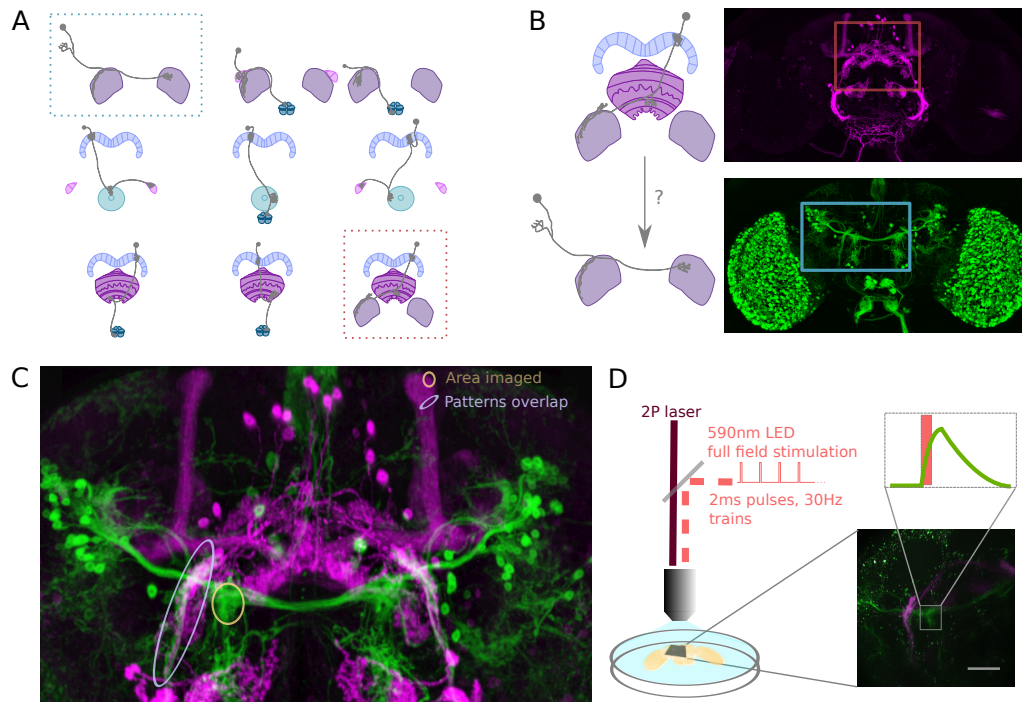
Figure S2: A functional connectivity screen. A: Schematics of a subset of the neurons considered for the screen. The example neurons shown in B and C are indicated by blue and orange dotted-line boxes. B: For each potential neuronal pair, driver lines with clean expression in the central complex were selected — the boxes delineate the approximate position of the neurons of interest in the brain. C: To determine if a given pair is a promising candidate, we examined the degree of overlap between the expression patterns in anatomy images registered to a common brain template. If the patterns overlapped (as indicated by the blue ellipse), we expressed CsChrimson in the presynaptic candidate, GCaMP6m in the postsynaptic candidate, and then imaged the ex-vivo brain in a 2-photon laser scanning microscope while optogenetically stimulating the presynaptic candidate population (D). We selected the region imaged based on proximity to the overlapping processes, but ensured that it contained only GCaMP expressing arbors (yellow ellipse in C).
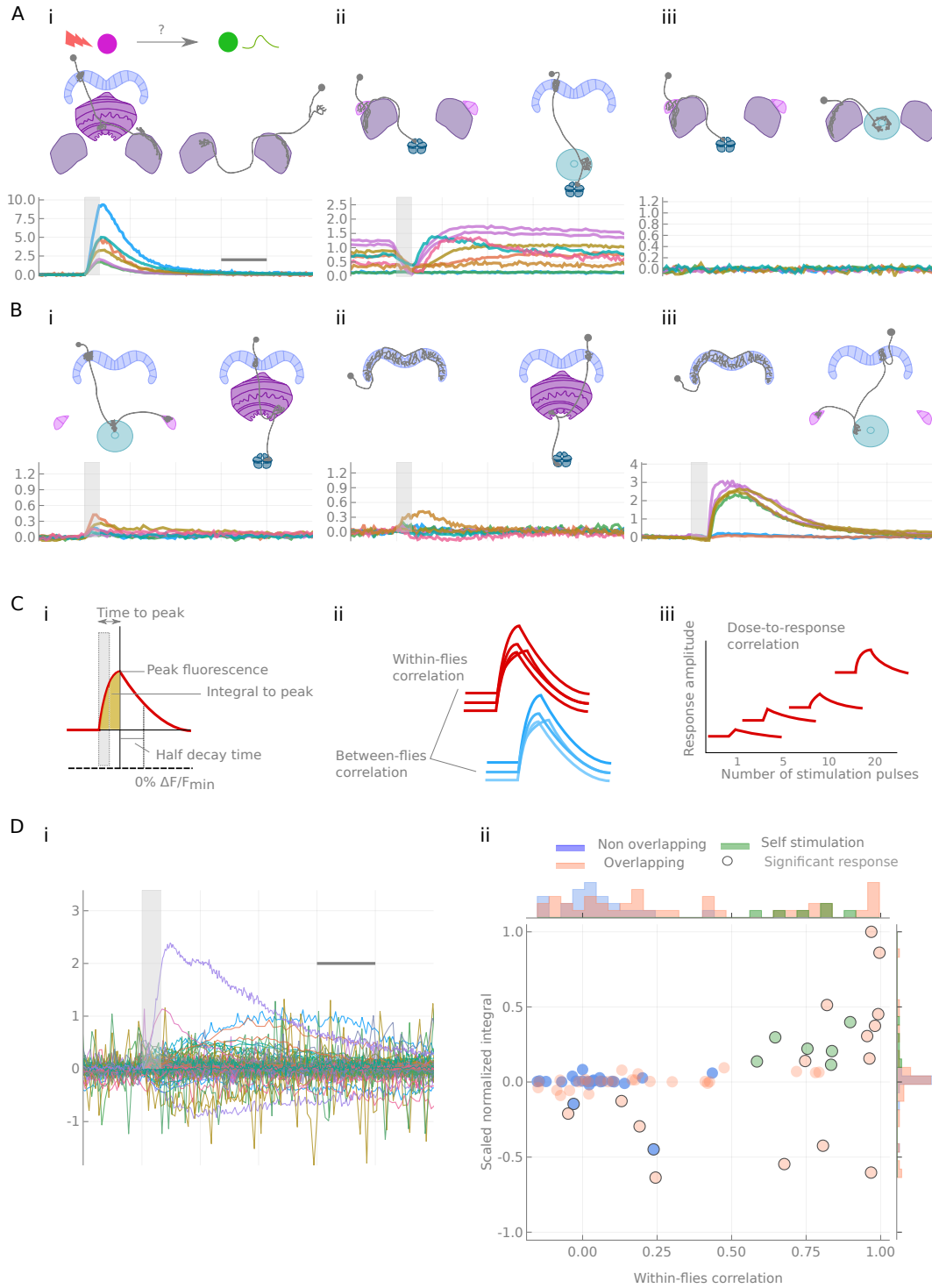
Figure S3: Characterization of calcium transients observed in response to optogenetic stimulation. A and B: Summary of different response types. Stimulation is indicated by the gray bar and consists of 20 light pulses (50 μW/mm^2, each of 2 ms duration) delivered at 30 Hz. A: Example neuron pairs, simple responses. (i) PF-LCre to SMPL-L. (ii) GL-N1 to P-EN1. (iii) GL-N1 to L-Ei. B: Example neuron pairs, unclear responses. (i) E-PG to P-F3N2d. (ii) Δ7 to P-F1N3. (iii) Δ7 to P-EG. In A and B, all responses, expressed as $\Delta F/F_0$, are baseline subtracted except for the inhibitory response in Aii. Scale bar 2 s. C: Example of statistics computed on individual runs and cell pairs characterizing: (i) average response shape, (ii) reliability of the response, and (iii) response sensitivity. D: Using the distribution of statistics from non-overlapping controls to assign classes to the responses: distributions of response amplitudes and reliability as measured by the scaled normalized integral (the median of the integral normalized to the baseline and scaled so that the dataset spans the [-1,1] range) and the between-flies correlation (see Materials and Methods). Each point corresponds to a different cell pair (median statistics across flies). Control unconnected pairs are shown in blue, and same-cell-type-stimulation in orange. Responses considered significantly different from the control

Figure S4: Anatomical and matrix representations of central complex connectivity. A: Diagrammatic representation. Solid lines indicate anatomically overlapping cell pairs, whereas dotted lines correspond to the non overlapping controls. The thickness of the lines maps to the functional connection strength. B: Matrix representation. Purple squares indicate the connections predicted from the anatomical overlaps. Connection strengths are quantified in terms of the Mahalanobis distance to the null sample, signed by the sign of the response integral and normalized to the maximum response. In A, the reliability of the responses as measured by the between-flies correlations is mapped to the transparency of the connectors.

Figure S5: Selected connectivity motifs within the central complex. A: Input channels. (i) Ring neurons provide inhibitory input to the E-PGs in the EB. (ii) GL-N1 inhibits P-EN neurons. (iii) Distributed excitatory input from IS-P neurons in the PB. B: $\Delta 7$ is probably the bottleneck in PB motifs, as it is the only strong post-synaptic target of E-PG neurons and relays information to other columnar neurons. C: The only output pair found so far connects the PF-LCre neuron to a LAL interneuron. D: Recurrence in the central complex. (i) at the input stage, and (ii) within the EB columnar system

Figure S6: Supplementary Figure related to Figure S2. Neuron types used, grouped by super-type.

Figure S7: Supplementary Figure related to Figure S3. Responses of non overlapping pairs. Each line corresponds to a fly, each color to a cell pair tested. Scale bar 2sec.
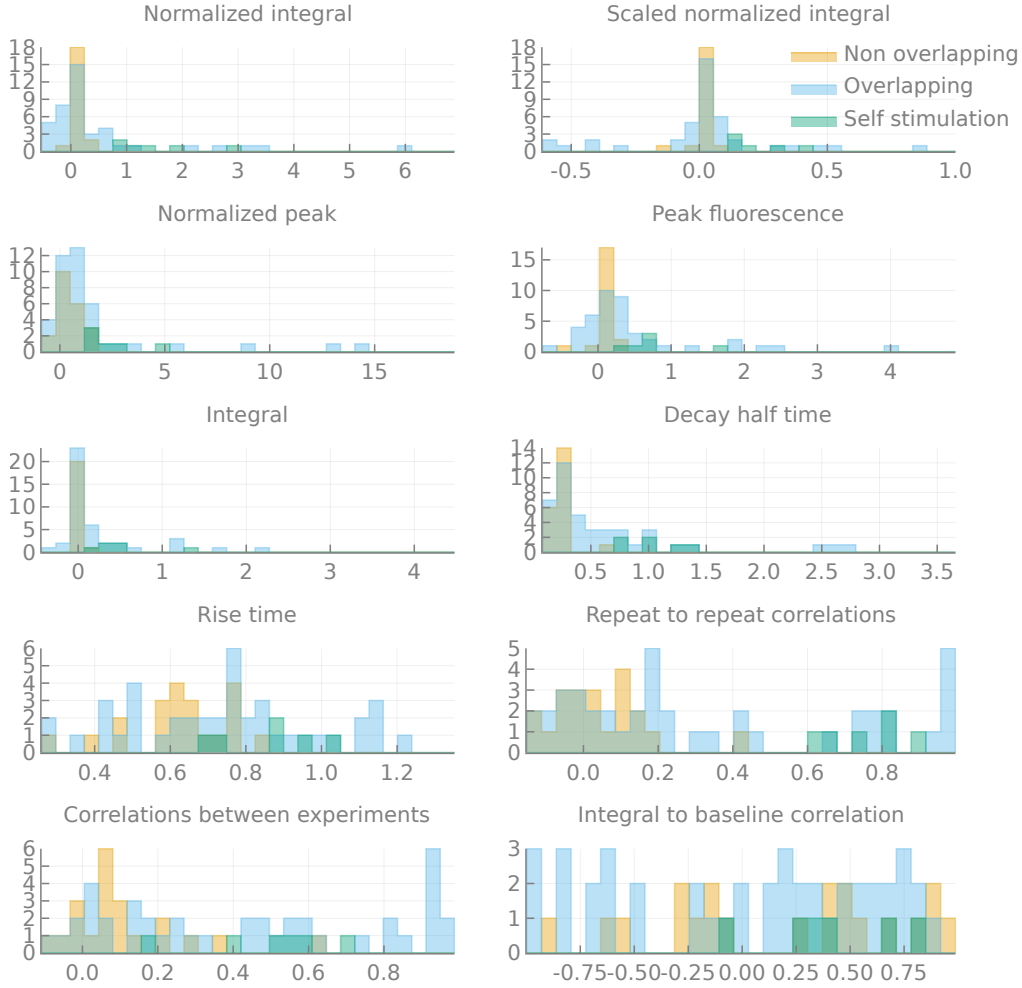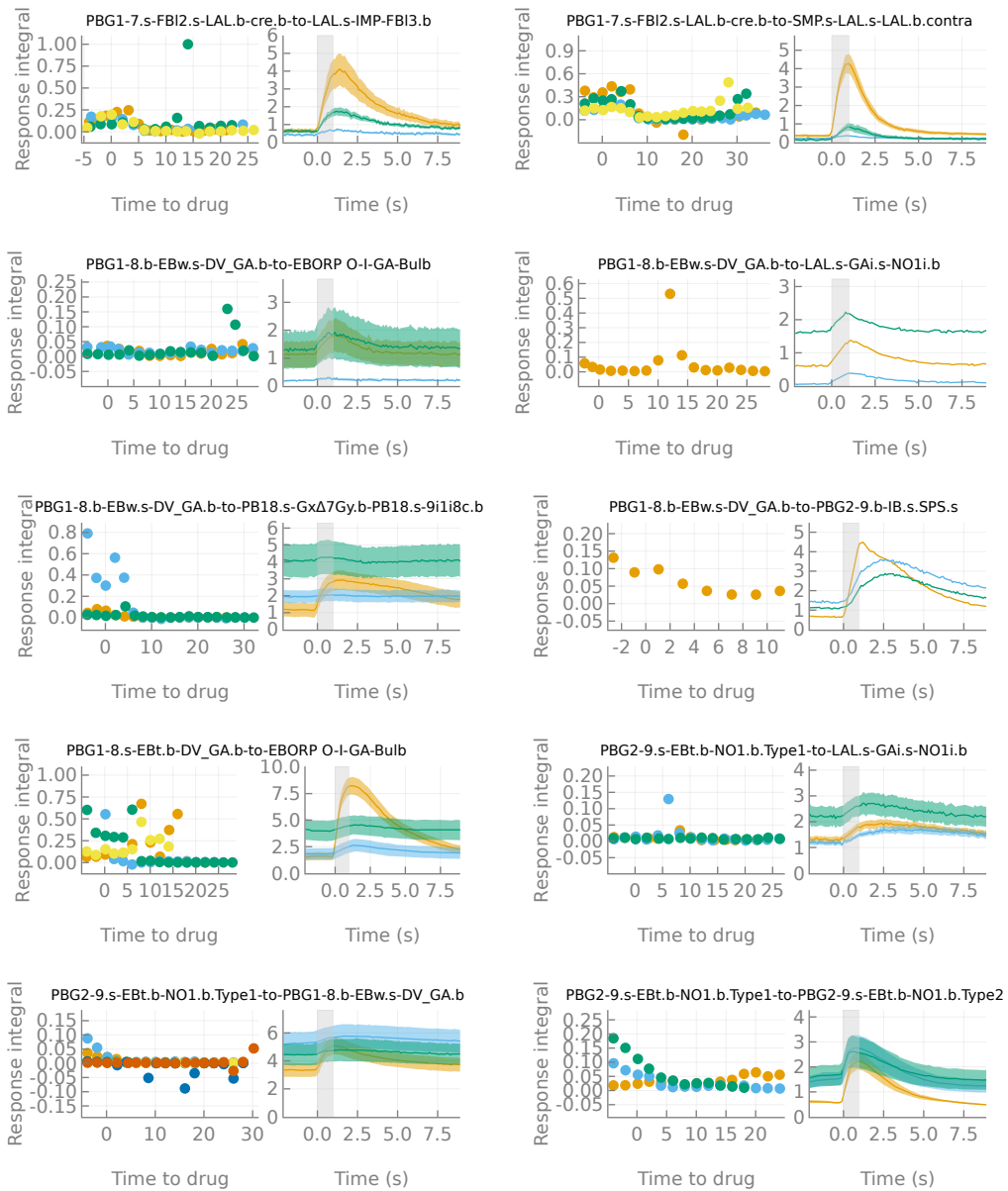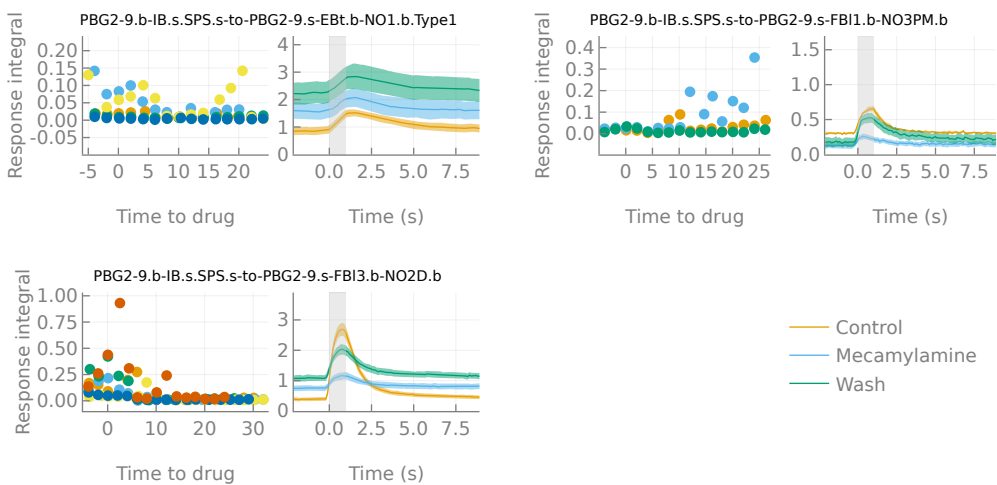

Figure S8: Supplementary Figure related to Figure S3. Distributions of statistics computed for non-overlapping, overlapping and self-activation pairs.
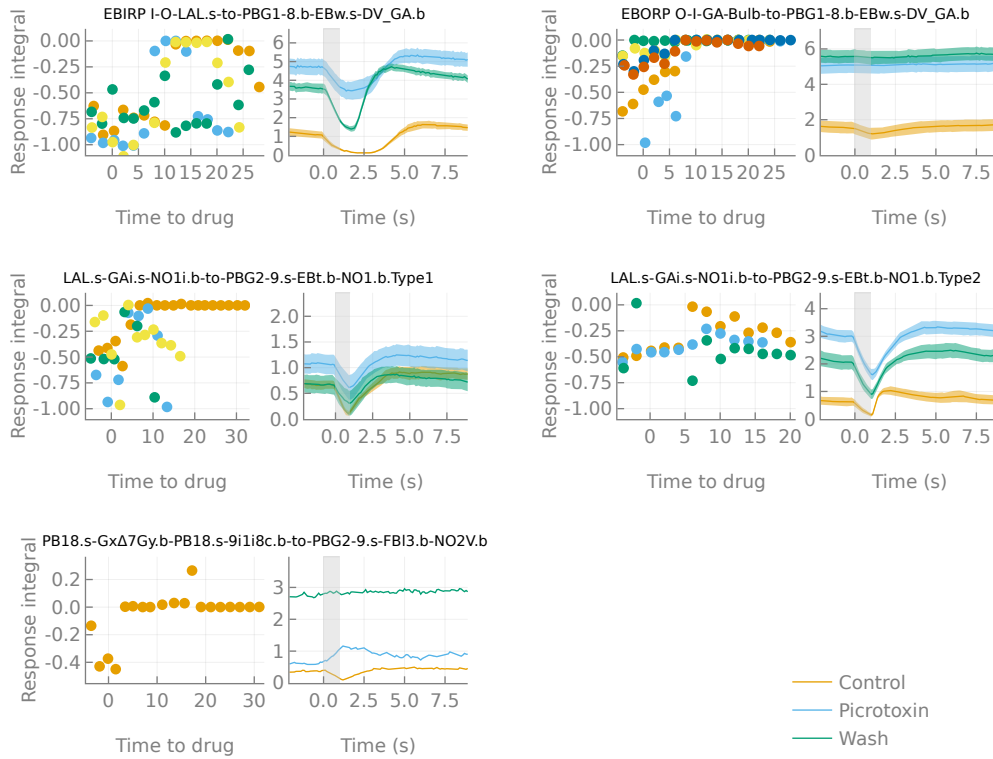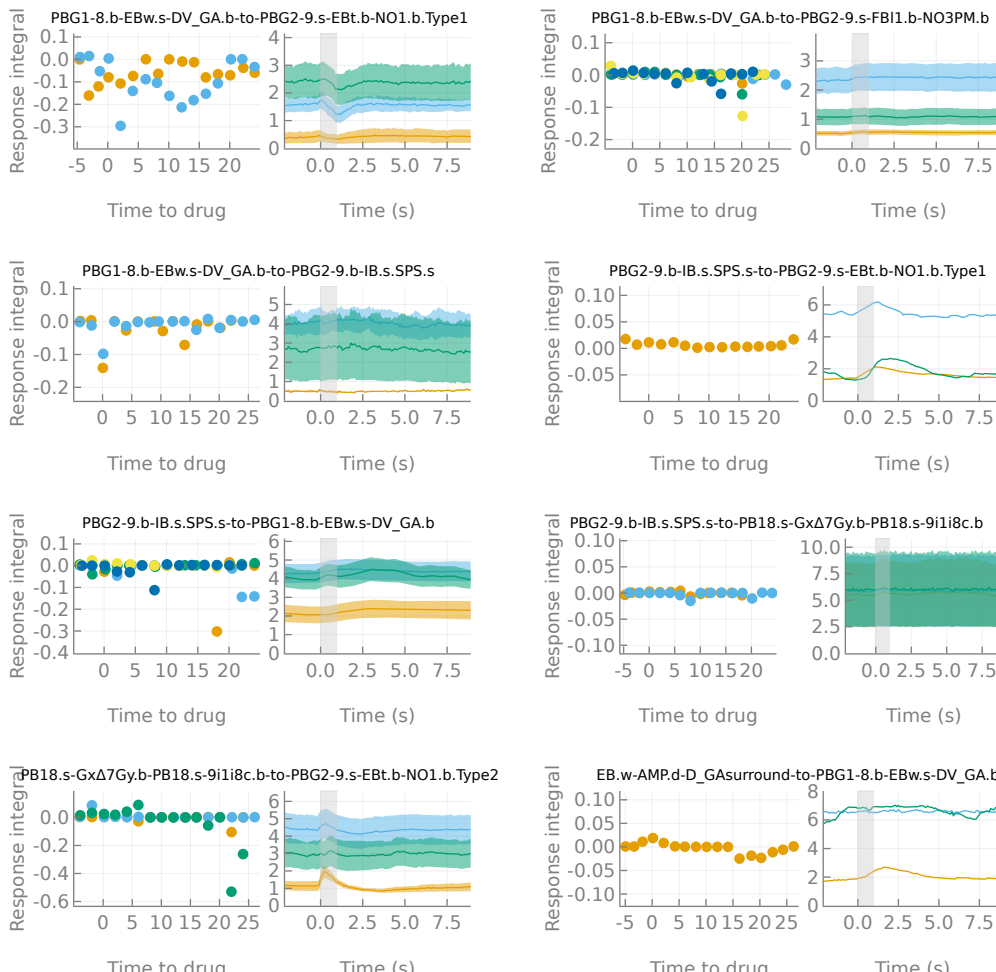
A

B

A

EBIRP I-O-LAL.s-to-PBG1-8.b-EBw.s-DV_GA.b

EBORP O-I-GA-Bulb-to-PBG1-8.b-EBw.s-DV_GA.b

LAL.s-GAi.s-NO1i.b-to-PBG2-9.s-EBt.b-NO1.b.Type1

LAL.s-GAi.s-NO1i.b-to-PBG2-9.s-EBt.b-NO1.b.Type2

PB18.s-GxΔ7Gy.b-PB18.s-9i1i8c.b-to-PBG2-9.s-FBl3.b-NO2V.b

Control
Picrotoxin
Wash

B

PBG1-8.b-EBw.s-DV_GA.b-to-PBG2-9.s-EBt.b-NO1.b.Type1

PBG1-8.b-EBw.s-DV_GA.b-to-PBG2-9.s-FBl1.b-NO3PM.b

PBG1-8.b-EBw.s-DV_GA.b-to-PBG2-9.b-IB.s.SPS.s

PBG2-9.b-IB.s.SPS.s-to-PBG2-9.s-EBt.b-NO1.b.Type1

PBG2-9.b-IB.s.SPS.s-to-PBG1-8.b-EBw.s-DV_GA.b

PBG2-9.b-IB.s.SPS.s-to-PB18.s-GxΔ7Gy.b-PB18.s-9i1i8c.b

PB18.s-GxΔ7Gy.b-PB18.s-9i1i8c.b-to-PBG2-9.s-EBt.b-NO1.b.Type2

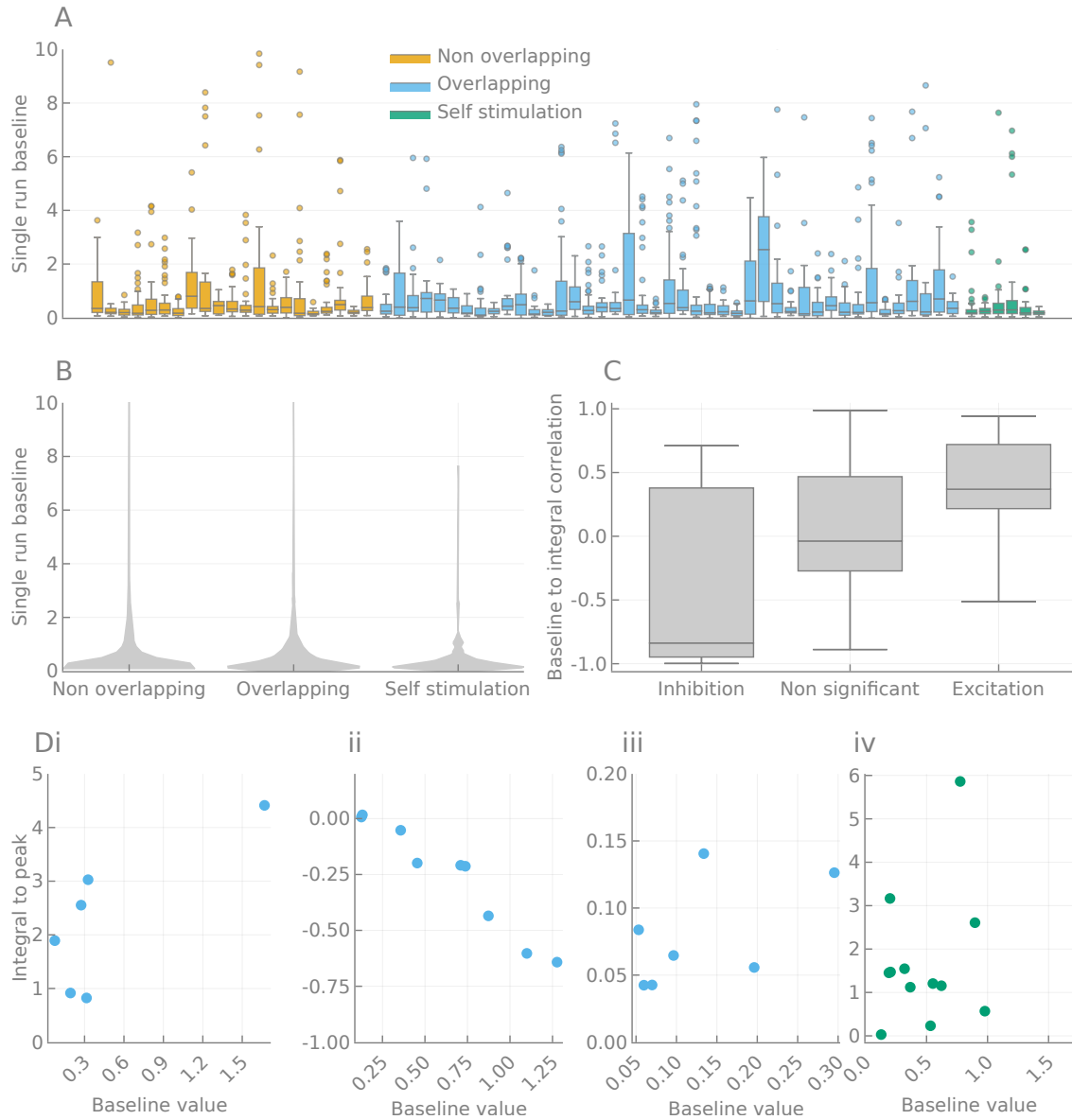EB.w-AMP.d-D_GAsurround-to-PBG1-8.b-EBw.s-DV_GA.b

Figure S11: Supplementary Figure: spread of fluorescence baseline, effect on the responses. A: Distribution of baseline fluorescence for each cell pair tested. Pairs are colored according to the "anatomical" class they belong to (overlapping, non-overlapping and self-activation). B: Same as A, but pooled by class. C: Correlations between the response signed distance and the baseline values of significantly responding pairs. Inhibitory responses are (as expected) correlated, but excitatory pairs also show a mild correlation. D: Example of distance to baseline relationship in 4 pairs. (i) PF-LCre to SMPL-L, corresponding to figure S3Ai. (ii) GL-N1 to P-EN1, corresponding to figure S3Aii. (iii) GL-N1 to L-Ei, corresponding to figure S3Aiii. (iv) PF-LCre to PF-LCre.
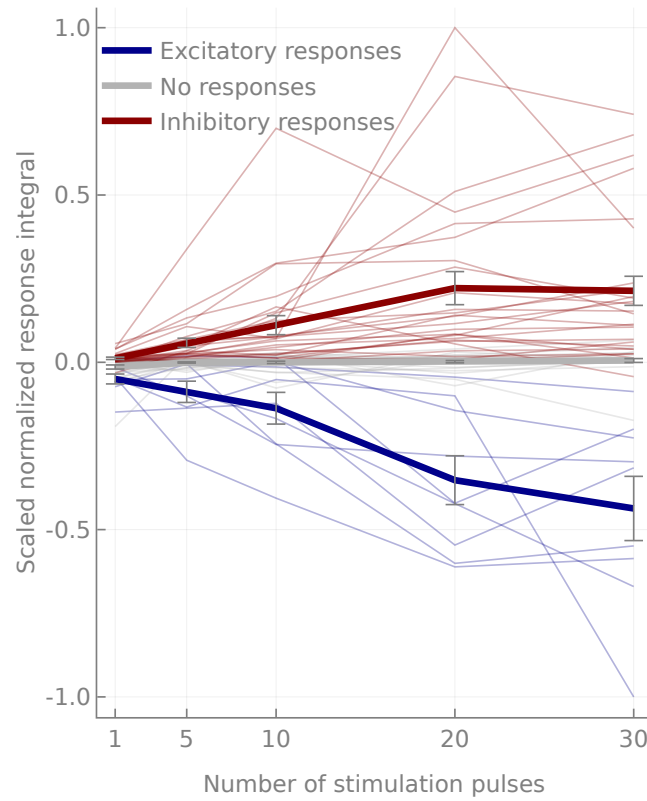
Figure S12: Supplementary Figure: dose responses. Thin lines correspond to median normalized scaled integrals of individual cell pairs. Cell pairs are grouped according to the class of their response (significantly excitatory/inhibitory or non significantly different from the controls). Note that both excitatory and inhibitory responses tend to saturate at 20 pulses.
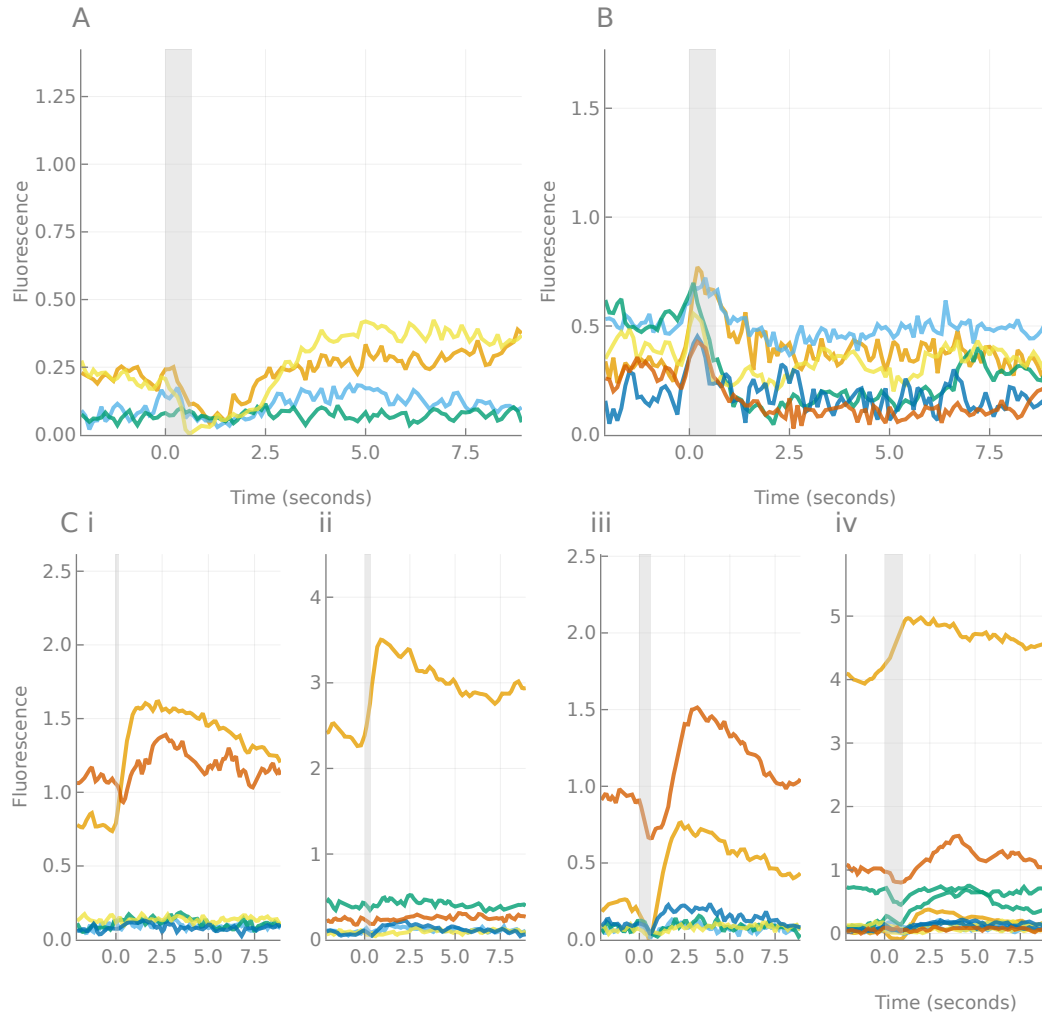
Figure S13: Various response types following $\Delta 7$ stimulations. A: $\Delta 7$ to P-F3N2v, inhibitory. B: $\Delta 7$ to P-EN1, excitatory. C: $\Delta 7$ to E-PG, mixed responses. (i) to (iv) correspond to 5, 10, 20 and 30 pulses stimulation protocol. Each line is the average response for one fly (four runs per fly).